J. Fluid Mech. (1992), *vol.* 238, *pp.* 657–682
Printed in Great Britain

Bénard convection in binary mixtures with Soret effects and solidification

By G. ZIMMERMANN[1]†, U. MÜLLER[1] AND S. H. DAVIS[2]

[1] Kernforschungszentrum Karlsruhe, Institut für Angewandte Thermo- und Fluiddynamik, Postfach 3640, W-7500, Karlsruhe, Germany

[2] Department of Engineering Sciences and Applied Mathematics, Northwestern University, Evanston, IL 60208, USA

(Received 17 December 1990 and in revised form 6 November 1991)

Bénard convection of a two-component liquid is considered. The liquid displays Soret effects and the boundary temperatures are fixed to span the solidification temperature of the mixture. Near the lower, heated plate the material is liquid and near the upper cooled plate there is a layer of pure solid solvent; all the solute is rejected during freezing. Linear stability theory is used to determine the effects on the critical conditions for Soret convection in the presence of the solidified layer and the interface between solid and liquid.

Experiments on mixtures of ethyl alcohol and water are performed using interferometry, photography and thermocouple measurements. The measured onset of instability to travelling waves at negative Soret coefficient compares well with those predicted by our linear theory. In the absence of ice the waves develop at finite amplitude to a fixed-amplitude state. However, when ice is present, these waves fail to persist but evolve to a state of steady finite-amplitude (overturning) convection. These differences are attributed to the presence of the ice and the nonlinear density profile of the basic state, both of which act as sources of non-Boussinesq effects.

1. Introduction

Convective mass transport in the liquid phase may determine the quality of technical materials when produced by controlled solidification. Typical examples are the growth of crystals from liquid solutions and the precision casting of ingots using directional solidification. The convection in the liquid, initiated by inhomogeneities of a temperature field, can change the local temperature and concentration fields at the liquid/solid interface, deform the interface, and thus influence the local solidification process which is itself controlled by diffusion (Kurz & Fisher 1989; Rosenberger 1979). The present investigation will focus on the possibility of unsteady convection in the liquid phase and its impact on the deformation of the liquid/solid interface.

A binary mixture subject to temperature gradients can generate concentration gradients as well. The Soret effect (Soret 1879; DeGroot & Mazur 1969) derives from the solute flux as a function of both gradients, so that an imposed temperature gradient can induce double-diffusive convection. The induced Soret solute flux may either add to or subtract from the imposed thermal gradient. In the latter case the opposing fields may generate oscillatory convective responses.

Single-phase convection in binary mixtures with negative Soret coefficient has

† Present address: Aachen Center for Solidification in Space, ACCESS e.V., Aachen, Germany.

been investigated intensively in the past two decades. Caldwell (1970, 1973, 1974) studies Bénard convection in sea water and finds a stabilizing effect of the thermal mass diffusion on the static state of heat conduction. From local temperature measurements within the layer he detects time-periodic temperature oscillations of small intensity when a critical condition for the static state is exceeded. For a fixed supercritical temperature difference the intensity and the period of oscillations increase monotonically in a transient phase until finally a permanent state of oscillatory convection is reached. Caldwell (1975, 1976) explores even smaller negative Soret coefficients using lithium–iodine solutions and observes similar phenomena.

Hurle & Jakeman (1971) and Platten & Chavepeyer (1972*a*, *b*) perform experiments in alcohol–water mixtures. They do not observe transient oscillatory states of varying frequency but describe stable permanent states of oscillatory convection of constant frequency.

Alcohol–water mixtures have proven particularly easy to handle and have been utilized by numerous investigators (Walden *et al.* 1985; Kolodner *et al.* 1986, 1987*a*, *b*; Surko *et al.* 1986; Ahlers, Cannell & Heinrichs 1987; Heinrichs, Ahlers & Cannell 1987; Steinberg, Moses & Fineberg 1987; Steinberg & Moses 1987; Fineberg, Moses & Steinberg 1988*a*, *b*, 1989; Bensimon *et al.* 1990) in their studies of the dynamics of convection in mixtures with Soret effects. In many of these recent experiments shadowgraphic methods have been employed to visualize the time-dependent behaviour of the cell pattern. The convection pattern is visualized from above through a transparent upper boundary of the test cell by generating shadowgraphs of the light reflected from the mirror polished bottom of the test cell. The main results from these experiments can be summarized as follows:

(i) Immediately after the onset of weak convection for slightly supercritical temperature differences across the layer, the roll pattern starts moving in the horizontal direction perpendicular to the roll axis. The convection presents itself as a travelling wave (Walden *et al.* 1985; Kolodner *et al.* 1986; Steinberg & Moses 1987; Moses, Fineberg & Steinberg 1987). The amplitude of the travelling waves may exhibit modulation (Heinrichs *et al.* 1987; Fineberg *et al.* 1988*a*, *b*).

(ii) The low-intensity state of travelling waves is unstable. In a transient period the intensity of the convective motion increases while the propagation speed of the wave motion decreases.

(iii) At the end of the transient period a stable, permanent state of travelling waves is observed characterized by a constant phase velocity (Moses & Steinberg 1986; Steinberg & Moses 1987).

(iv) If the temperature difference across the layer is increased, the phase velocity of the stable state of travelling waves decreases. At another higher value of the temperature difference a smooth transition to steady convection, often called overturning convection, occurs (Linz *et al.* 1988; Moses & Steinberg 1986; Steinberg & Moses 1987; Ahlers & Rehberg 1986; Rehberg & Ahlers 1986; Sullivan & Ahlers 1988*a*, *b*).

In some of the cited experimental work cells of small lateral extent were used. A clear picture of the various travelling-wave effects is not always obtained, mainly because of the uncontrolled generation of and the interaction of travelling-wave patterns at different locations in the cell. This experimental deficiency is largely eliminated by the annular type test cell used by Kolodner, Bensimon & Surko (1988*a*) and Bensimon *et al.* (1990). Their test cell eliminates end effects in the azimuthal direction and so avoids azimuthal wave reflections. These experiments

realize travelling wave packets in both azimuthal directions. They observe modulated travelling waves generated by the interaction of wave packets of slightly different wavelength. They also find a permanent finite-amplitude state of azimuthally travelling waves of uniform intensity. Similar observations have been made by Heinrichs *et al.* (1987) and Ahlers *et al* (1987) in rectangular test cells in which one horizontal dimension is the largest of the box. Long-range material transport due to wave action has been identified by Moses & Steinberg (1988) by adding photochromic tracers to the liquid.

Zimmermann (1990) and Zimmermann & Müller (1992) investigate linear and nonlinear convective phenomena in binary mixtures of ethyl alcohol and water in a shallow rectangular cell with one lateral dimension much longer than the other. They employ differential interferometry to visualize the density-gradient field, and thermocouples to sense the temperature fluctuations inside the liquid layer. They study the structure of the travelling waves, and the generation and reflection processes of the travelling waves at the ends of the test cell. They observe stable travelling-wave modes, consistent with earlier studies, as long as the mean temperature of the fluid is much larger than the solidification temperature T_s of the mixture. However, when the mean temperature of the fluid is near enough to T_s, the travelling waves are not permanent, but undergo a transition to steady (overturning) convection. They attribute these changes to the presence at low temperatures of significant nonlinearities in the density–temperature profile of the basic state.

The stability of the static state of a binary mixture with Soret effect was first studied theoretically by Hurle & Jakeman (1969, 1971). Further investigations of this problem have been conducted by Platten (1971), Schechter, Prigogine & Hamm (1972), Legros, Platten & Poty (1972) and Platten & Chavepeyer (1972*a*, *b*). These authors base their stability analyses on the simplifying assumption that the concentration profile of the static state is linear and the separation ratio, characterizing the Soret effect, is constant everywhere in the mixture. Chock & Li (1975) solve the linear stability problem for a complete set of balance equations, describing the transport processes in mixtures. There are a number of more recent analyses, e.g. Linz & Lücke (1987), Zielinska & Brand (1987), Knobloch & Moore (1988) and Cross & Kim (1988). The essential result of the linear stability analyses can be summarized in terms of the Soret coefficient S as a measure of the intensity of thermal mass. There is a critical value S^* of S such that $S^* < 0$. There are two cases that occur when the temperature difference across the layer exceeds a critical value. When $S > S^*$, the static state is replaced by a state of steady convection. When $S < S^*$, a state of oscillatory convection occurs. At $S = S^*$ both convective states merge at a codimension-two point.

Weakly nonlinear theories for finite-amplitude convection in binary mixtures have been developed by Cross (1986*a*) and Ahlers & Lücke (1987). Although these authors assume stress-free and solute-permeable boundaries in their eight-mode model equations they do predict some typical dynamical features like travelling waves, modulated travelling waves, instability of standing waves, and variations of the frequency with amplitude as observed in experiments. Linz & Lücke (1987) have improved the eight-mode model by satisfying the zero-solute-flux condition at the boundaries. Wave interaction has been included in a nonlinear analysis by Brand, Lomdahl & Newell (1986) and Brand & Steinberg (1984). They suggest that spatially irregular, oscillatory convection patterns observed in some experiments can be explained via a Benjamin–Feir instability. The effect of finite test-cell geometry on travelling wave convection has been investigated numerically by Deane, Knobloch

& Toomre (1988) and analytically by Cross (1986*b*, 1988). They find quiescent regions and standing wave patterns, respectively, in the neighbourhood of walls perpendicular to the direction of wave propagation for slightly supercritical heating conditions.

The influence of Bénard convection on the liquid–solid interface in a partially solidified *single-component* layer has been studied by Davis, Müller & Dietsche (1984), Dietsche (1984), Dietsche & Müller (1985) and Grauer & Haken (1988). Experiment and weakly nonlinear theory show that beyond a certain critical temperature difference across the layer the static state of heat conduction is replaced in the liquid phase by convection in the form of rolls, if the solid layer is thin, and by convection in form of hexagonal cells, if the solid layer is thick. The thickness of the solid affects the thermal properties of the solid–liquid interface and hence affects the preferred mode of convection.

In the present work we consider Bénard convection of a binary mixture in which the temperatures of the horizontal boundaries span the solidification temperature of the mixture. There is a steady basic state in which the layer is partly liquid and partly solid, the interface between these is planar, and in which all transport is by conduction and diffusion. We examine the case in which the solidifying material completely rejects the solute so that the solid is pure solvent. We then examine the linear stability of the basic state and determine how the presence of solid and the ability of the material to solidify or melt under disturbance affects the critical conditions for the onset of instability. We then examine experimentally water–ethyl alcohol mixtures for their onset properties. Both the theory and experiment are compared to cases when phase change is absent and to cases where phase change is present but Soret effects are absent. The experiment further probes the finite-amplitude state to which the system tends.

2. Theory

2.1. *Formulation*

Consider the configuration sketched in figure 1 in which a pair of horizontal parallel plates of infinite horizontal extent are separated by a distance h, and acceleration due to gravity of magnitude g is directed downward. The lower plate at $z = 0$ is fixed at the temperature $T = T_0$ while the upper plate at $z = h$ is fixed at temperature $T = T_1$. The material between the plates is a two-component liquid if $T > T_s$ and pure solid if $T < T_s$. Thus, the lean component is completely rejected when the liquid solidifies at the melting temperature T_s. The layer is heated uniformly from below such that $T_1 < T_s < T_0$, so there is a solid–liquid interface at $z = \eta$ with $0 < \eta < h$. The (constant) material properties are the density ρ_0, the specific heat c_p, the thermal conductivity λ, thermometric conductivity κ, kinematic viscosity ν, and volume expansion coefficients α and α' for thermal and concentration effects, respectively. The lean component has diffusivity D and Soret coefficient S_0. The sign of S_0 is consistent with Platten & Legros (1984). For $S_0 > 0$ the more dense component diffuses toward the cold upper boundary. Superscripts S and L will be used to designate, respectively, solid and liquid properties when required.

2.2. *Differential equations and boundary conditions*

The coupled effects of buoyancy-driven convection and phase changes will be described by thermal conduction in the solid and the Boussinesq equations in the liquid.

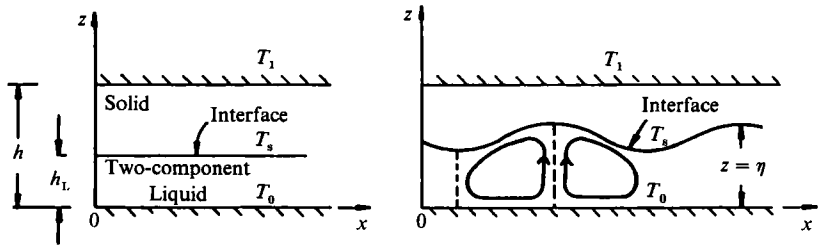

FIGURE 1. Schematic drawing of a partially solidified layer.

We have in the solid

$$T_t^{(S)} = \kappa^{(S)} \nabla^2 T^{(S)}, \tag{2.1a}$$

and in the liquid

$$\boldsymbol{v}_t + \boldsymbol{v}\cdot\nabla\boldsymbol{v} = -\frac{1}{\rho_0^{(L)}}\nabla p + \nu\nabla^2\boldsymbol{v} + [\alpha(T^{(L)} - T_{s0}) + \alpha' C^{(L)}]\, g\,\boldsymbol{k}, \tag{2.1b}$$

$$\nabla\cdot\boldsymbol{v} = 0, \tag{2.1c}$$

$$T_t^{(L)} + \boldsymbol{v}\cdot\nabla T^{(L)} = \kappa^{(L)}\nabla^2 T^{(L)}, \tag{2.1d}$$

$$C_t^{(L)} + \boldsymbol{v}\cdot\nabla C^{(L)} = -\nabla\cdot\boldsymbol{j}, \tag{2.1e}$$

where

$$\boldsymbol{k} = (0, 0, 1). \tag{2.1f}$$

We have used a linear equation of state for the density in the buoyancy term of (2.1*b*) and T_{s0} is a reference temperature to be defined shortly.

At the interface at $z = \eta$, we ignore capillary undercooling (the Gibbs–Thomson effect) so that

$$T^{(L)} = T^{(S)} = T_s. \tag{2.2}$$

The jump in heat flux is balanced by the production of latent heat L:

$$\rho^{(S)} L\eta_t = [\lambda^{(S)}\nabla T^{(S)} - \lambda^{(L)}\nabla T^{(L)}]\cdot\boldsymbol{n}N, \tag{2.3}$$

where $\boldsymbol{n}$ is the unit normal vector to the interface,

$$\boldsymbol{n} = (-\eta_x, -\eta_y, 1)N^{-1}, \tag{2.4a}$$

and

$$N = (1 + \eta_x^2 + \eta_y^2)^{\frac{1}{2}}. \tag{2.4b}$$

Subscripts x, y, z, t represent partial differentiation. The common temperature T_s of the interface, defined in (2.2), is unknown *a priori* since it depends on the concentration $C^{(L)}$ (defined in mole fraction, say) of the lean component at the interface. We write the equilibrium relation, depicting the phase behaviour, in a linear form:

$$T^{(L)} = T_{s0} = T_{s1} + m' C^{(L)}. \tag{2.5a}$$

Here m is the slope of the melting curve of an ideal mixture which is given by

$$m' = -RT_{s1}^2/L \tag{2.5b}$$

with R being the universal gas constant, L the heat of fusion of the solvent and T_{s1} its melting temperature. The lean-component mass balance at the interface takes the form

$$\rho^{(S)} C^{(L)}\eta_t = \rho_0^{(L)}\boldsymbol{j}\cdot\boldsymbol{n}N, \tag{2.6}$$

since the concentration of the lean component in the solid is zero. Here the flux $\boldsymbol{j}$, allowing for Soret diffusion, takes the form

$$\boldsymbol{j} = -D[\boldsymbol{\nabla} C^{(\mathrm{L})} - S_0 C^{(\mathrm{L})}(1-C^{(\mathrm{L})})\,\boldsymbol{\nabla} T^{(\mathrm{L})}]. \tag{2.7}$$

where S_0 is the Soret number. The interface is non-mobile but deformable so that there is the kinematic condition

$$N\rho_0^{(\mathrm{L})}\boldsymbol{v}\cdot\boldsymbol{n} = (\rho_0^{(\mathrm{L})} - \rho_0^{(\mathrm{S})})\,\eta_t \tag{2.8}$$

and the no-slip conditions

$$\boldsymbol{v}\cdot\boldsymbol{t}^{(1)} = \boldsymbol{v}\cdot\boldsymbol{t}^{(2)} = 0, \tag{2.9}$$

where $\boldsymbol{t}^{(1)}$ and $\boldsymbol{t}^{(2)}$ are unit tangent vectors

$$\boldsymbol{t}^{(1)} = (1+\eta_y^2, -\eta_x\eta_y, \eta_x)\,(1+\eta_y^2)^{-\frac{1}{2}}N^{-1}, \tag{2.10a}$$

$$\boldsymbol{t}^{(2)} = (0, 1, \eta_y)\,(1+\eta_y^2)^{-\frac{1}{2}}. \tag{2.10b}$$

At the upper plate at $z = h$, the temperature is fixed:

$$T^{(\mathrm{S})} = T_1. \tag{2.11}$$

At the lower plate at $z = 0$, the temperature is fixed, and the plate is rigid and impermeable:

$$T^{(\mathrm{L})} = T_0 \tag{2.12a}$$

$$\boldsymbol{v} = \boldsymbol{0}, \tag{2.12b}$$

$$\boldsymbol{j}\cdot\boldsymbol{k} = 0. \tag{2.12c}$$

The equation (2.12c) gives the vanishing of the mass flux of the lean component.

In order to define the mass of the lean component we imagine the whole layer to be occupied at time $t = 0$ by a homogeneous two-component liquid with concentration C_0. When the layer is partially solidified, there is the overall mass balance for this component,

$$C_0 h = \frac{1}{\mathscr{A}}\int_{\mathscr{A}}\int_0^{\eta} C^{(\mathrm{L})}\,\mathrm{d}z\,\mathrm{d}\mathscr{A} \tag{2.13}$$

where $\mathscr{A}$ represents the horizontal area of one spatial period in the convection. The z-integration interval reflects the absence of the lean component in the solid.

2.3. *Static solution*

The governing system possesses a static solution in which the interface is planar at $z = \eta = h_{\mathrm{L}}$, the velocity vector $\boldsymbol{v}$ is identically zero, the pressure p is hydrostatic and the temperatures are purely conductive. Here

$$\bar{T}^{(\mathrm{L})} = T_{\mathrm{s}0} - (T_0 - T_{\mathrm{s}0})\frac{z-h_{\mathrm{L}}}{h_{\mathrm{L}}} \tag{2.14a}$$

and

$$\bar{T}^{(\mathrm{S})} = T_{\mathrm{s}0} - (T_{\mathrm{s}0} - T_1)\frac{z-h_{\mathrm{L}}}{h-h_{\mathrm{L}}}. \tag{2.14b}$$

Fields (2.14) satisfy conditions (2.2), (2.11) and (2.12a). The flux condition (2.3) further constrains the parameters so that

$$\frac{h_{\mathrm{S}}}{h_{\mathrm{L}}} = \frac{\lambda^{(\mathrm{S})}}{\lambda^{(\mathrm{L})}}\frac{T_{\mathrm{s}0}-T_1}{T_0-T_{\mathrm{s}0}} \equiv A \tag{2.15}$$

where
$$h = h_S + h_L; \tag{2.16}$$

we call A the height ratio. The absolute temperatures of the boundaries determine the fraction of solid present. Here T_{s0} is the (concentration-dependent) interface temperature T_s in the basic state. To determine the value of T_{s0} and hence the temperature gradients, we must find $\bar{C}^{(L)}$. We solve (2.1*e*) and (2.7) subject to condition (2.12*c*) and find that

$$\bar{C}_z^{(L)} - S_0 \bar{C}^{(L)}(1-\bar{C}^{(L)})\,\bar{T}_z^{(L)} = 0. \tag{2.17}$$

This automatically satisfies condition (2.6). The solution of (2.17), given $\bar{T}^{(L)}$ from (2.14*a*), is

$$\bar{C}^{(L)} = \left\{1 + \frac{1-\bar{C}^{(L)}(h_L)}{\bar{C}^{(L)}(h_L)} \exp\left[\frac{T_0 - T_{s0}}{h_L} S_0 (z - h_L)\right]\right\}^{-1}, \tag{2.18}$$

where the constant of integration, the interface concentration $\bar{C}^{(L)}(h_L)$ is determined through the conservation law (2.13). We obtain from

$$C_0 h = \int_0^{h_L} \bar{C}^{(L)}\,\mathrm{d}z \tag{2.19}$$

that
$$\bar{C}^{(L)}(h_L) = \frac{\exp\left[\dfrac{T_0 - T_{s0}}{h_L} S_0 h C_0\right] - 1}{\exp\left[\dfrac{T_0 - T_{s0}}{h_L} S_0 h_L\right] - 1}. \tag{2.20}$$

Given $\bar{C}^{(L)}$, we have from (2.5*a*) the interface temperature T_{s0},

$$T_{s0} = T_{s1} + m' \bar{C}^{(L)}(h_L). \tag{2.21}$$

Thus, the thickness of the solid and liquid layers is determined by T_0, T_1, T_{s0} and C_0. In particular, as $A \to 0$, the solid disappears.

2.4. *Dimensionless equations*

The equations (2.1) and the interfacial conditions (2.3) and (2.5)–(2.8) can be transformed into a dimensionless form by introducing the following scales:

$$\left.\begin{aligned} x, y, z \sim h_L, \quad t \sim h_L^2/\kappa^{(L)}, \quad u, v, w \sim \kappa^{(L)}/h_L, \\ p \sim \rho_0^{(L)} \nu \kappa^{(L)}/h_L^2, \quad T - T_{s0} \sim T_0 - T_{s0}, \quad C^{(L)} \sim C_0. \end{aligned}\right\} \tag{2.22}$$

The resulting dimensionless Boussinesq equations and interfacial conditions contain the following set of non-dimensional numbers:

$$R = \frac{\alpha g (T_0 - T_{s0}) h_L^3}{\kappa^{(L)} \nu}, \quad R_s = \frac{\alpha' g h_L^3}{D\nu}, \quad A = \frac{\lambda^{(S)}}{\lambda^{(L)}} \frac{T_{s0} - T_1}{T_0 - T_{s0}}, \tag{2.23a–c}$$

$$P = \frac{\nu}{\kappa^{(L)}}, \quad Sc = \frac{\nu}{D}, \quad \rho = \frac{\rho_0^{(S)}}{\rho_0^{(L)}}, \quad \lambda = \frac{\lambda^{(S)}}{\lambda^{(L)}}, \quad \kappa = \frac{\kappa^{(S)}}{\kappa^{(L)}}, \tag{2.23d–h}$$

$$St = \frac{\rho_0^{(L)} L \kappa^{(L)}}{\lambda^{(L)} (T_0 - T_{s0})}, \quad S = S_0 (T_0 - T_{s0}), \quad m = \frac{m'}{T_0 - T_{s0}}, \quad C_0. \tag{2.23i–l}$$

The basic state (2.14)–(2.21) can also be written in non-dimensional terms as follows:

$$T^{(\mathrm{L})} = 1-z, \quad T^{(\mathrm{S})} = \lambda^{-1}(1-z), \tag{2.24a, b}$$

$$\frac{h}{h_{\mathrm{L}}} - 1 = \frac{h_{\mathrm{S}}}{h_{\mathrm{L}}} = \lambda \frac{T_{\mathrm{s0}} - T_{\mathrm{I}}}{T_0 - T_{\mathrm{s0}}} \equiv A, \tag{2.24c}$$

$$\bar{C}^{(\mathrm{L})} = \left\{ C_0 + \frac{1 - C_0 \bar{C}^{(\mathrm{L})}(1)}{\bar{C}^{(\mathrm{L})}(1)} \exp\left[S(1-z)\right] \right\}^{-1}, \tag{2.24d}$$

where

$$\bar{C}^{(\mathrm{L})}(1) = \frac{\exp\left[(1+A)\,SC_0\right] - 1}{\exp\left[S\right] - 1} \frac{1}{C_0}. \tag{2.24e}$$

Given the value of $\bar{C}^{(\mathrm{L})}(1)$, (2.21) determines the (dimensional) interface temperature T_{s0} used in the scaling.

2.5. *Linear stability theory*

We perturb the governing non-dimensional system about the static basic state (2.25) and we introduce normal modes for each disturbance quantity ϕ' as follows:

$$\phi'(x, y, z, t) = \Phi(z) \exp\left[-\omega t + \mathrm{i}(k_1 x + k_2 y)\right], \tag{2.25a}$$

where

$$k = (k_1^2 + k_2^2)^{\frac{1}{2}} \tag{2.25b}$$

and introduce the velocity components

$$\boldsymbol{v}' = (u', v', w'). \tag{2.26}$$

We denote d/dz by D. In the following $(W, T^{(\mathrm{L})}, T^{(\mathrm{S})}, C^{(\mathrm{L})}, H)$ are the z-dependent normal-mode amplitudes of the corresponding disturbance quantities. We eliminate u', v', p' from the momentum equations by cross-differentiation to obtain

$$(\mathrm{D}^2 - k^2)\,(\mathrm{D}^2 - k^2 + \omega P^{-1})\,W - k^2[RT^{(\mathrm{L})} + R_{\mathrm{s}} PSc^{-1} C_0 C^{(\mathrm{L})}] = 0. \tag{2.27a}$$

From the heat transport equation and the transport equation for the lean component we get

$$(\mathrm{D}^2 - k^2 + \omega)\,T^{(\mathrm{L})} + W = 0, \tag{2.27b}$$

$$-\mathrm{D}J - k^2[C^{(\mathrm{L})} - S\bar{C}^{(\mathrm{L})}(1 - C_0 \bar{C}^{(\mathrm{L})})\,T^{(\mathrm{L})}] + \omega ScP^{-1} C^{(\mathrm{L})} - ScP^{-1} \bar{C}_z^{(\mathrm{L})}\,W = 0, \tag{2.27c}$$

where

$$-J = \mathrm{D}C^{(\mathrm{L})} - S[\bar{C}^{(\mathrm{L})}(1 - C_0 \bar{C}^{(\mathrm{L})})\,\mathrm{D}T^{(\mathrm{L})} - (1 - 2C_0 \bar{C}^{(\mathrm{L})})\,C^{(\mathrm{L})}]. \tag{2.27d}$$

In the solid, the heat conduction equation gives

$$(\mathrm{D}^2 - k^2 + \omega\kappa^{-1})\,T^{(\mathrm{S})} = 0. \tag{2.28}$$

The linearized boundary conditions for the ordinary differential equations (2.27) and (2.28) are as follows:

on $z = 0$,

$$T^{(\mathrm{L})} = W = \mathrm{D}W = J = 0; \tag{2.29}$$

on $z = 1 + A$,

$$T^{(\mathrm{S})} = 0; \tag{2.30}$$

on $z = 1$,

$$T^{(\mathrm{S})} - T^{(\mathrm{L})} = -H(1 - \lambda^{-1}), \tag{2.31a}$$

$$-\omega\rho StH = \lambda \mathrm{D}T^{(\mathrm{S})} - \mathrm{D}T^{(\mathrm{L})}, \tag{2.31b}$$

$$T^{(\mathrm{L})} - H = mC_0[C^{(\mathrm{L})} + H\bar{C}_z^{(\mathrm{L})}(1)], \tag{2.31c}$$

$$-\omega\rho ScP^{-1} \bar{C}^{(\mathrm{L})} H = \boldsymbol{j}' \cdot \boldsymbol{k} \equiv J \tag{2.31d}$$

$$-\omega(1-\rho)\,H = W, \tag{2.31e}$$

$$\mathrm{D}W = 0. \tag{2.31f}$$

We solve (2.28) subject to the conditions (2.30) and (2.31) and obtain

$$T^{(S)}(z) = [T^{(L)} + (\lambda^{-1} - 1)\, H]\, \tilde{A}(\zeta), \tag{2.32a}$$

where

$$\zeta = \frac{z-1}{A}, \quad \tilde{A} = \frac{\sinh \delta A(1-\zeta)}{\sinh \delta A}, \tag{2.32b, c}$$

and

$$\delta = (k^2 - \omega\kappa^{-1})^{\frac{1}{2}}. \tag{2.32d}$$

We now evaluate condition (2.31*b*), using (2.32), and eliminate H by using condition (2.31*c*). We obtain

$$\mathrm{D}T^{(L)} + \{\mathscr{L}[1 + \lambda m C_0 \bar{C}^{(L)}(1)] - \omega\rho St\}\{1 + mC_0 \bar{C}_z^{(L)}(1)\}^{-1} T^{(L)} - mC_0[\mathscr{L}(1-\lambda) - \omega\rho St]\{1 + mC_0 \bar{C}_z^{(L)}(1)\}^{-1} C^{(L)} = 0. \tag{2.33a}$$

Here

$$\mathscr{L} = -A^{-1} \frac{\mathrm{d}}{\mathrm{d}\zeta} \tilde{A}(\zeta)|_{\zeta=0} = \delta \coth \delta A. \tag{2.33b}$$

Condition (2.31*d*), using (2.31*c*), becomes

$$J = -\omega\rho Sc P^{-1} \bar{C}^{(L)}[T^{(L)} - mC_0 C^{(L)}][1 + mC_0 \bar{C}_z^{(L)}]^{-1}. \tag{2.33c}$$

Condition (2.31*e*), using (2.31*c*), becomes

$$W + \omega(1-\rho)[T^{(L)} - mC_0 C^{(L)}][1 + mC_0 \bar{C}_z^{(L)}]^{-1} = 0, \tag{2.33d}$$

while (2.31*f*) remains

$$\mathrm{D}W = 0. \tag{2.33e}$$

The result of the linear stability analysis is a system of differential equations for the normal-mode amplitudes in the fluid and expressions for the corresponding boundary conditions at $z = 0$ and 1. The boundary-value problem defined by (2.27), (2.29) and (2.33) is solved numerically using the SUPORT code of Scott & Watts (1975); see Zimmermann, Müller and Davis (1986) for details.

2.6. *Numerical results*

The numerical results in this section are obtained for a set of parameters typical for organic mixtures like cyclohexane–benzene. We use $P = 17.6$, $Sc = 1047$, $R_s = 28.4$, $St = 5.91$, $m = -80$, $\kappa = \lambda = \rho = 1.001$. Here $R_s = (T_0 - T_1)^{-1}\alpha'/\alpha$.

2.6.1. *The effect of diffusion and conduction*

We first examine the pure Soret-convection problem in which the layer is all liquid and no solidified material is present; thus $A = 0$. Figure 2 shows for $C_0 = 0.01$, the critical Rayleigh number, wavenumber and angular frequency as functions of S.

When $S = 0$, there is no Soret effect and instability sets in as steady Bénard convection with $R_c^{(s)} = 1708$, $k_c^{(s)} = 3.117$ and $\omega_c = 0$. Here ω_c is the value at critical of the imaginary part of the ω in (2.25*a*). When $S > 0$, the instability is still steady, $\omega_c = 0$, and both $R_c^{(s)}$ and $k_c^{(s)}$ decrease with S, consistent with the results of Chock & Li (1975). When $S > 0$, the Soret diffusion moves the more dense component toward the cold boundary reinforcing the adverse density gradient. When $S < 0$, the opposite is the case and instability is opposed by Soret effects, as shown in figure 2 and in the results of Chock & Li (1975). In addition, when S is sufficiently negative $S < S^* < 0$, a new instability mode, periodic in time, occurs. The corresponding critical Rayleigh number $R_c^{(p)}$ is smaller than $R_c^{(s)}$ for each S. The $k_c^{(p)}$ is slightly smaller than $k_c^{(s)}$ while the frequency ω_c of this oscillatory mode decreases with S with

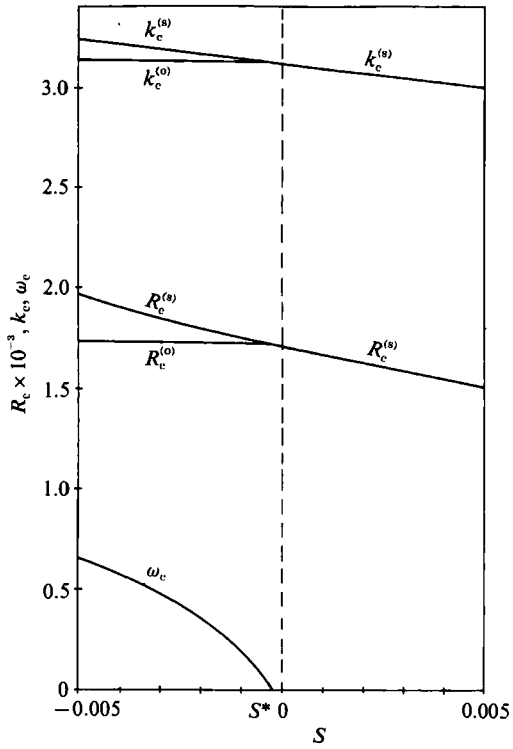

FIGURE 2. Critical Rayleigh number R_c, wavenumber k_c, critical angular frequency ω_c, as a function of the Soret number S for an initial concentration $C_0 = 0.01$, and height ratio $A = 0$. S^* denotes a codimension-two point.

$\omega_c \to 0$ as $S \to S^*$. Thus, the steady and periodic modes merge as $S \to S^*$, resulting in a codimension-two point at $S = S^*$. The present calculations give $S^* = -0.00025$. In general $R_c^{(p)}$, $k_c^{(p)}$ and ω_c all increase with $|S|$ for $S < S^*$. Platten & Legros (1984) discuss how S^* depends on P, Sc and R_s. The appearance of the oscillatory mode is the result of a double-diffusive mechanism in which the temperature and concentration distributions oppose each other and where their fields diffuse with vastly different time scales, τ_T and τ_C, respectively. Since $\tau_T \ll \tau_C$, a warm fluid element that rises in the layer loses its temperature contrast in a time τ_T well before its concentration contrast decays. The parcel thus becomes too heavy for its environment, and falls into a warmer layer. If this slower process is on a timescale τ_C, the density of the parcel adjusts to its surroundings, the parcel becomes lighter and rises again due to thermal buoyancy. The cycle then begins anew. Thus, the phase lag between thermal and solute diffusion leads to an over-compensating restoring force, which is responsible for the oscillatory mode.

2.6.2. *The effect of initial concentration*

We again examine the pure Soret-convection problem in the absence of solidified material but for different initial concentrations C_0. Figure 3 shows how R_c, k_c and ω_c depend on C_0. All curves cross at $S = 0$ where Soret effects are absent. $R_c^{(s)}$ decreases with C_0 for $S > 0$ as expected since more of the lean component is present to participate in Soret diffusion. Again, as expected, $k_c^{(s)}$ decreases with C_0 for fixed $S > 0$. When $S < S^*$ and the instability is oscillatory for fixed S all the quantities

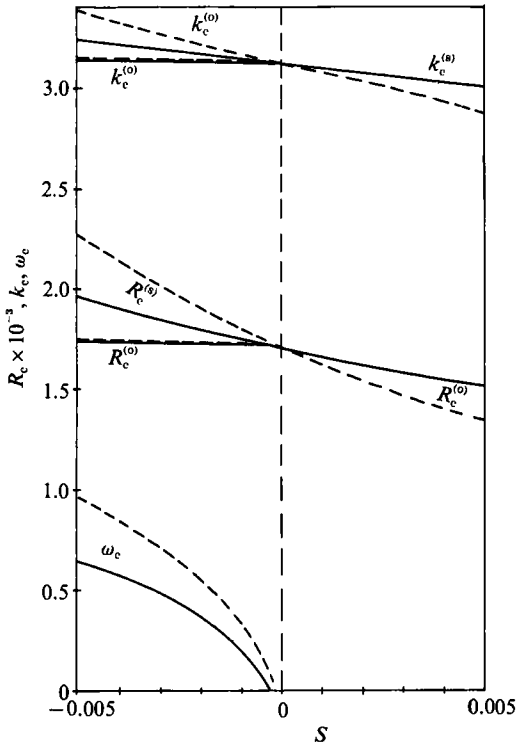

FIGURE 3. Critical Rayleigh number R_c, wavenumber k_c and angular frequency ω_c, as a function of the Soret number S for the initial concentrations $C_0 = 0.01$ (solid line) and $C_0 = 0.02$ (dashed line), and height ratio $A = 0$.

$R_c^{(o)}$, $k_c^{(o)}$ and ω_c increase with C_0. More detailed calculations (see Zimmermann *et al.* 1986) show that both $R_c^{(o)}$ and $k_c^{(o)}$ increase nearly linearly with C_0 for $C_0 > 0.02$. The above results are consistent with the idea that an increase in C_0 effectively increases S. As can be seen from (2.27*c*, *d*), Soret diffusion enters the governing equations through a term of the form $S\bar{C}^{(L)}[1 - C_0\bar{C}^{(L)}]$. The numerical calculations for $A = 0$ show that $\bar{C}^{(L)}$ is nearly linear in the range $|d\bar{C}^{(L)}/dz| < 10^{-3}$. Thus, $\bar{C}^{(L)} \sim C_0$ and if $C_0^2 \ll 1$, then

$$S\bar{C}^{(L)}[1 - C_0\bar{C}^{(L)}] \approx SC_0 = S_{eff}. \tag{2.34}$$

An increase of C_0 is equivalent to an increase in $|S|$, consistent with the results of figure 3. Note that (2.27*d*) has a second term dependent upon S. Given the above argument, it becomes independent of C_0.

2.6.3. *The effect of the solidified layer*

When the layer is partially solidified, $A > 0$ and all of the lean component has been rejected into the liquid. Figure 4 gives the critical conditions for $C_0 = 0.01$, and for the cases $A = 0$ (reproduced from figure 2) and $A = 1$. When $S = 0$, Soret diffusion is absent and there is thermal conduction in the solid and conduction and convection in the liquid. This case was treated by Davis *et al.* (1984). They find that the presence of the solidified layer affects the thermal environment seen by the thermal perturbations in the liquid. When $A = 0$, the upper boundary of the liquid is a perfect conductor and as A increases, the heat transfer properties of this upper boundary deteriorate. Thus, the thicker the solid layer the lower the R_c for the onset of

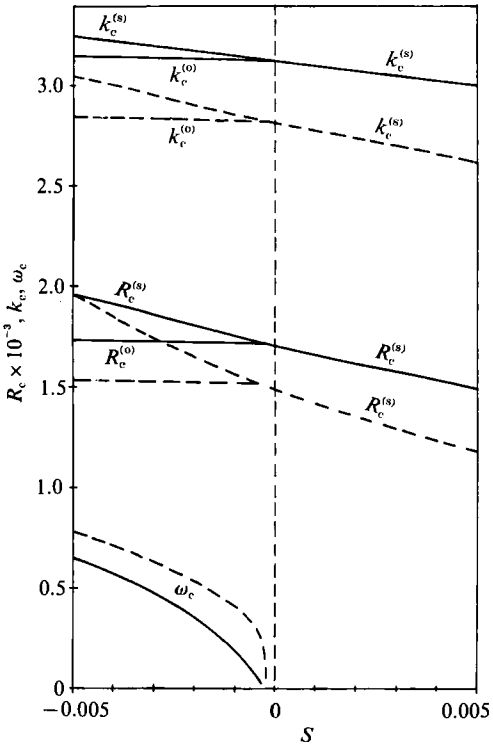

FIGURE 4. Critical Rayleigh number R_c, wavenumber k_c and angular frequency ω_c, as a function of the Soret number for the initial concentration $C_0 = 0.01$ and height ratios $A = 0$ (solid line) and $A = 1$ (dashed line).

convection. This is seen for $S = 0$ in figure 4 where one finds $R_c^{(s)}|_{A=1} < R_c^{(s)}|_{A=0}$. We saw earlier that, in the absence of a solidified layer, $R_c^{(s)}$ decreases with S. Thus, the two effects reinforce each other. We see that by making $S < 0$ and greater in magnitude the Soret effect stabilizes and hence there is a cross-over point ($S \approx -5 \times 10^{-3}$ for $A = 1.0$) where the two effects balance and $R_c^{(s)}$ has the same value as for $A = 0$.

The above behaviour derives from the property that the solid rejects lean component so that for a given C_0 its actual concentration in the liquid is greater the thicker the solid layer. Given the above approximation for $\bar{C}^{(L)}$, (2.24*e*) implies that $\bar{C}^{(L)} \approx (1+A)C_0$ so that now

$$S_{\text{eff}} \approx SC_0(1+A). \tag{2.35}$$

Thus, if $A = 1$, we have effectively doubled C_0 or equivalently S.

In summary, when $S < 0$, an increase in C_0 stabilizes the basic state, which is further enhanced by the increase in A. When $S > 0$, the basic state is destabilized by the increase of A. This destabilizing effect of increasing ice thickness for $S > 0$ is also found by Hadji & Schell (1990) in their recent calculations.

2.6.4. *The effect of the latent heat*

The latent heat affects the system in two ways: directly through the rate of solidification or melting via the Stefan condition (2.3); and indirectly through its influence on m, because m varies inversely proportionally to L, (2.5*b*), by modifying the melting temperature of the solid.

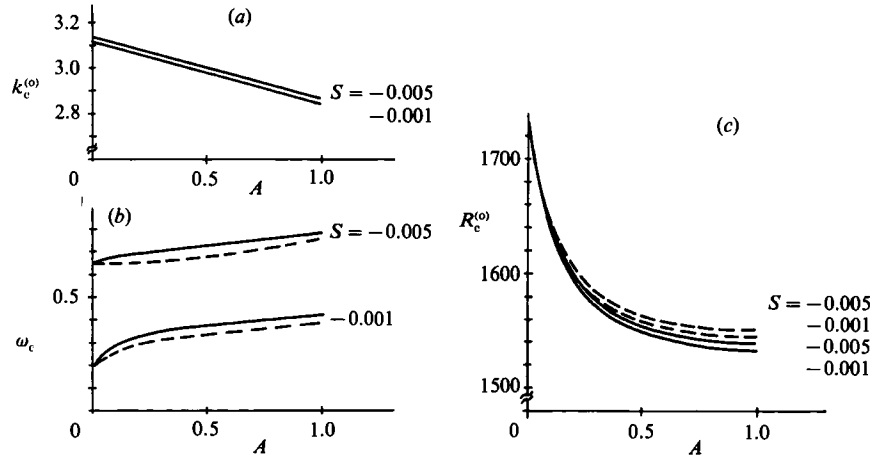

FIGURE 5. Critical (*a*) wavenumber k_c, (*b*) angular frequency ω_c and (*c*) Rayleigh number R_c as a function of the height ratio A for the initial concentration $C_0 = 0.01$ for the two Soret numbers $S = -0.001$ and 0.005, and for two different Stefan numbers $St = 5.91$ (solid lines) and 11.82 (dashed lines).

We now double the value of the latent heat used in the pressure calculations: L is changed from 31.3 to 62.6 kJ/kg. The calculations show that the marginal curves of $R_c^{(s)}$ and $k_c^{(s)}$ are changed by less than 0.1%. This occurs via the modification of m by latent heat through changes in T_{s0}, (2.5*a*, *b*). This variation of T_{s0} is very small ($< 1\%$) for the considered ranges of C_0 and A.

Figure 5 shows the effect of the enhanced latent heat on the marginal curves $R_c^{(o)}$, $k_c^{(o)}$ and ω_c. The calculations have been performed for $C_0 = 0.01$, a range of A, and for two values of the Soret number $S = -0.001$ and -0.005. The graphs show that $R_c^{(o)}$ is only slightly increased and $k_c^{(o)}$ is practically unchanged when the latent heat is doubled (see figure 5*a*, *c*). However, a noticeable decrease of the angular frequency ω_c is found. This effect is stronger for negative values of S and $|S|$ large. It depends, moreover, on A and C_0 (figure 5*b*).

During the oscillatory convection, local solidification and melting occurs at the interface. In the local freezing and melting process larger amounts of heat must be transported by conduction in the solid for higher values of the latent heat. This requires more time under externally fixed thermal boundary conditions. Hence, the increase of L should decrease ω_c.

In summary, an increased latent heat influences only slightly the critical Rayleigh number and the wavenumber, though the angular frequency decreases noticeably.

3. Experiments

3.1. *Experimental techniques*

The experiments are performed in a test apparatus, which is similar to the one described by Dietsche & Müller (1985) and sketched in figure 6. A rectangular test volume of aspect length:width:height = 200:20:3.12 mm, is chosen in order to foster the generation of regular-roll convection patterns. The volume is demarked by two copper blocks which serve as the upper and lower boundaries. Crystal glass plates form the long sidewalls. Two Teflon blocks are placed between the copper

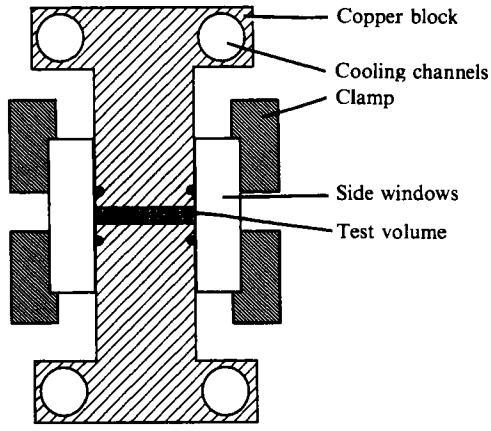

FIGURE 6. Cross-section of the test apparatus.

blocks and simultaneously serve as spacer elements and the shorter sidewalls. O-rings are employed to seal off the cavity. The copper blocks are heated or cooled by circulating temperature-controlled coolant from thermostats through jackets at the upper and lower end of the two blocks. The overall design of the test apparatus is based on three-dimensional heat-conduction calculations that provide to a very good approximation a linear temperature distribution across the cavity in the pre-convective state. According to calculations, horizontal-temperature inhomogeneities are less than 0.1 % at the ends of the long sides and less than 0.01 % otherwise. Nearly ideal temperature conditions before onset of convection are needed to investigate the transition to oscillatory flow, since even the smallest convective motions, due to temperature inhomogeneities, may disturb significantly the concentration profiles in the layer. The test apparatus is insulated externally by a Styrofoam cover all of which is placed in an air-conditioned chamber with good temperature control. The air temperature in this chamber is kept at the mean temperature, $T = \frac{1}{2}(T_0 + T_1)$, of the test liquid during the experiments. This procedure proved to be necessary for tests with solidification at temperatures significantly lower than the laboratory temperature.

The selection of a suitable test liquid is crucial for a clear experimental identification of the phenomena. For our experiments the following requirements had to be met: a sufficiently negative value of the Soret coefficient, good transparency of the liquid for employing visualization technique, near-ideal liquid solution with constant physical properties and a linear density–temperature –concentration dependence (i.e. Boussinesq properties), solidification of pure material (complete rejection of solute) when the temperature falls below the liquidus temperature.

After thorough pretests employing cyclohexane–benzene mixtures and ethyl alcohol–water mixtures the latter was chosen as a test liquid mainly because of its strong Soret effects. Alcohol–water mixtures have been used frequently in the past by, among others, Hurle & Jakeman (1971, 1973*a*, *b*), Villers & Platten (1984) and Lhost & Platten (1988, 1989). The physical properties of this mixture are well documented in the literature. In particular the effective Soret number S_{eff} which characterizes the thermal diffusion effect can be varied between negative and positive values by changing the concentration of the solute (see Kolodner, Williams & Moe 1988*c*) and the mean temperature in the test liquid. Moreover, only pure water is solidified from such dilute mixtures.

Just as pure water has a density maximum at 4 °C, low-concentration alcohol–water mixtures may have such maxima near their solidification temperatures T_s. They occur for alcohol concentrations $C < 14$ wt % but not otherwise, though even for $C > 14$ wt % the mixture may still have nonlinear density profiles in the basic state. The solute concentration affects T_{s0} and hence the scaling for S, (2.23j). Increasing the solute concentration shifts the operating point for negative S toward S^*, which leads to oscillations of both low frequency and intensity. As a compromise, a mixture of 15 wt % ethyl alcohol and water is used in all experiments with partially solidified layers. According to D'an-Lax (1967), $T_s = -7.6$ °C.

The mixture of water and ethanol fulfils the requirement that the solute is completely rejected from the solid phase. Ott, Goates & Waite (1979) measured the phase diagram of water–ethanol very precisely, and for concentrations of ethanol used in our experiments, find that the solidified material is pure-water ice.

The quality of the measurement is determined by the long-term constancy of the temperatures at the upper and the lower boundaries of the test cavity. These temperatures are controlled by two high-precision Haake thermostats of a coolant outlet-temperature variance $\Delta T = \pm 0.01$ °C. At low temperatures ethyl alcohol is used as a coolant. The thermostats are connected to the test apparatus by plastic hoses isolated by thick rubber-foam wrappings.

The flow in the cooling channels of the test apparatus is counter current. The temperatures in the copper blocks are measured by precision platinum-resistance thermometers which are threaded through bore holes in the copper blocks very close to the boundaries of liquid layer. The measuring arrangement used determines the temperature difference across the layer to an accuracy of $\delta(\Delta T) = \pm 0.002$ K. The quality of the temperature control of the test apparatus may be judged by the fact that for static or stable-flow conditions in the liquid layer the measured temperature difference is constant up to $\delta(\Delta T) = \pm 0.003$ K.

The temperature fluctuations within the liquid layer are measured by a NiCr–Ni thermocouple of 0.25 mm in diameter protruding 0.9 mm into the test volume from the lower copper boundary. The thermocouple is located at the centre of this boundary. The voltage between this thermocouple and a reference thermocouple in the lower copper block is recorded. This voltage is amplified and further processed to give signals of the temperature oscillations T' in test liquid as a pen-chart record. The resolution of the temperature oscillations is $\delta T' = \pm 0.02$ K. From the chart records the period τ of periodic temperature fluctuation can be evaluated by averaging over a sequence of 20 periods to an accuracy of $\delta\tau/\tau \approx 0.01$.

The convective flow in the test volume is visualized by employing a differential interferometer (see Bühler, Kirchartz & Srulijes (1978), Kirchartz (1980) for an outline of the technique). In general the differential interferometer generates lines of constant density difference in the direction of the beam separation. If the separation length e is small as in the present case, $e = 0.3$ mm, lines of constant density difference become lines of constant temperature gradient. The interferometer beams integrate the density differences only in one direction through the test volume, as is the case in the present set-up (see figure 6). A quantitative evaluation of the fringe pattern is only possible for perfectly two-dimensional flow. Since experiments with corrugated interfaces have significant three-dimensional disturbances, we use the interferograms for qualitative information only. In the present experiment only horizontal beam splitting is used. Bühler (1979) has shown for slightly supercritical conditions that the fringe pattern generated from horizontal beam splitting can be interpreted to a good approximation as the streamline pattern for two-dimensional

convection patterns. The interferograms are recorded by a high-resolution video camera. Further processing is performed by employing a digital image-processing system. Each interferogram shown in figure 8 shows a segment of 43 mm of the 200 mm test volume. In order to take interferograms from each part of the test volume the interferometer is placed on an optical bench that can be moved transversely in a controlled manner. When there are moving cellular patterns, quantitative determination of wavelengths and the direction of the pattern movement can be made if one examines interferograms taken at distinct time intervals.

The thickness of the ice layer is measured and photographed with the aid of a mobile stereomicroscope. Using magnifications of up to 22 times, the liquid-layer height is determined to an accuracy of $\Delta h_L = \pm 0.02$ mm. Since the height ratio and Rayleigh number are based on the liquid-layer height, they, too, are affected by errors of the same order.

3.2. *Experimental results*

We begin by summarizing briefly our observations from tests with liquid mixtures without ice. In this case the mean temperature in the test volume is well above the solidification temperature T_s of the test liquid. These observations will be needed later for comparison with the partially solidified layer. For more details see the Zimmermann (1990), and Zimmermann & Müller (1992).

If the temperature difference across the layer is raised quasi-steadily, the static state of heat conduction becomes unstable and convection starts in the form of a moving cellular pattern. This pattern is commonly interpreted as a travelling wave (TW) (see e.g. Walden *et al.* 1985; Moses & Steinberg 1986; Linz *et al.* 1988). The interferograms show that under fully developed conditions roll cells with axes parallel to the shorter side of the test cell move from one end of the cell to the other. Owing to small temperature inhomogeneities, the roll cells are first generated at the ends of the test volume and propagate towards the centre. The moving roll cells are sensed by the thermocouple in the cell centre as a time-periodic temperature fluctuation. For Rayleigh numbers near critical the temperature signal shows time-modulated amplitudes which increase exponentially, though, slowly with time. The growth rates depend on the amount by which the Rayleigh numbers exceed the critical value. During this period of the developing TW-convection, the observed oscillation frequency is constant. When the intensity of the TW-convection, as characterized by the amplitude of the oscillating temperature signal, exceeds a threshold value, the modulated TW-convection mode saturates via a short transient to a permanent oscillatory state of constant amplitude. During this short transient, the period of oscillation increases typically from $\tau = 37$ to 500 s for a mixture of a concentration $C_0 = 15$ wt% and a mean temperature $\bar{T} = 10$ °C, thus indicating the nonlinear character of this transition. The experiments show, furthermore, that the state of permanent finite-amplitude travelling waves exists only in a limited range of Rayleigh numbers in which the period of oscillation increases monotonically with increasing Rayleigh number.

If the Rayleigh number is increased quasi-steadily past a second critical value $R_2 (R_2 = 1.59 R_c$ for $C_0 = 15$ wt%, and $\bar{T} = 10$ °C), the permanent travelling wave becomes unstable and a jump transition (see e.g. Moses & Steinberg 1986 and Surko *et al.* 1986) leads the system to a stable state of steady convection (commonly called overturning convection). The transitions from the static state to the stable travelling wave and at higher Rayleigh numbers from travelling waves to steady convection are hysteretic, indicating that both states may originate from subcritical bifur-

cations.† Experiments conducted at lower mean temperatures of the liquid and for lower initial concentrations show that the range of Rayleigh numbers in which permanent travelling waves can be observed shrinks. If with $C_0 = 15$ wt% the mean temperature of the layer is reduced below $\bar{T} = 5$ °C, a permanent state of travelling waves is not observed. Rather, at the onset of convection the transient state of modulated travelling waves evolves directly to a steady-state convection. It is conjectured by Zimmermann (1990) and Zimmermann & Müller (1992) that the significantly nonlinear density–temperature relation destabilizes the travelling wave when the temperatures are near T_s.

Density measurements show that mixtures with ethanol concentrations less than 14 wt% have, like pure water, a maximum in the density. By using an ethanol concentration of 15 wt%, this anomaly can be avoided, though the density still depends nonlinearly on the temperature.

To estimate such non-Boussinesq effects, it is necessary to know the temperature dependence of the density. From data given by D'an-Lax (1967) for the temperature range $-5 < T < 30$ °C we get for a mixture with $C_0 = 15$ wt% ethanol thermal-expansion coefficients of $\alpha = 0.000238\ \mathrm{K}^{-1}$ at $T = 10$ °C and $\alpha = 0.000188\ \mathrm{K}^{-1}$ at 5 °C; this constitutes a decrease of about 27%.

Another indication of non-Boussinesq behaviour is given by our experiments done at $T = 10$ and 5 °C. The reduced Rayleigh numbers for the onset of the travelling waves (without ice) are, respectively, 1.27 and 1.89. These values correspond to critical temperature differences of 11.5 and 22 °C. The higher temperature differences required to destabilize the heat-conducting state at lower mean temperatures are largely attributable to the nonlinearity of the density profile.

We now turn to experiments on partially solidified layers of ethyl alcohol–water mixtures with $C_0 = 15$ wt%. We start with the *static basic state* of heat conduction and thermal mass diffusion. The temperature T_1 of the upper copper block of the test cell is lowered quasi-steadily below T_s of the mixture, producing a thin ice layer at the top of the liquid layer. By adjusting T_1 in the range $T_s = -7.6 > T_1 > -16.65$ °C, ice layers of thicknesses $h_s, 0 < h_s < 0.87$ mm, are generated. Next, the temperature T_0 of the lower boundary is raised in several small steps of up to $\Delta T = 0.4$ K. The temperature increase per step is conducted over a period of 30 min. Several hours are left between each step in order to assure local thermal equilibrium everywhere in the test volume. When the critical temperature difference $\Delta T_c^{(L)}$ in the liquid layer is exceeded, convection is observed in the form of modulated travelling waves (MTW). Figure 7 shows a typical signal of the temperature oscillations recorded by the thermocouple in the cell centre. In this case the basic-state thickness of the ice layer is $h_s = 0.11 \pm 0.02$ mm.

A temperature increase at the lower boundary from $T_0 = 16.49$ to 16.97 °C in 30 min triggers the TW-convection mode at one corner of the test cell. As in the case of TW-convection in layers without ice, new convection rolls of varying intensity and wavelength are consecutively formed at the particular corner of the test cell pushing the previously formed rolls ahead towards the cell centre and beyond. As a result of this generation process, a modulated wave train whose amplitude grows in time travels through the liquid layer from one end of the test cell to the other. Given fixed

† Recently, Kolodner *et al.* (1988*a*) have demonstrated by their experiments in annular containers that the jump transition, as well as the hysteresis effect, for the transition from travelling waves to overturning convection and vice versa is related to the pinning of the convection rolls by the endwalls of finite test cells. For their annular test cell they do not observe these features.

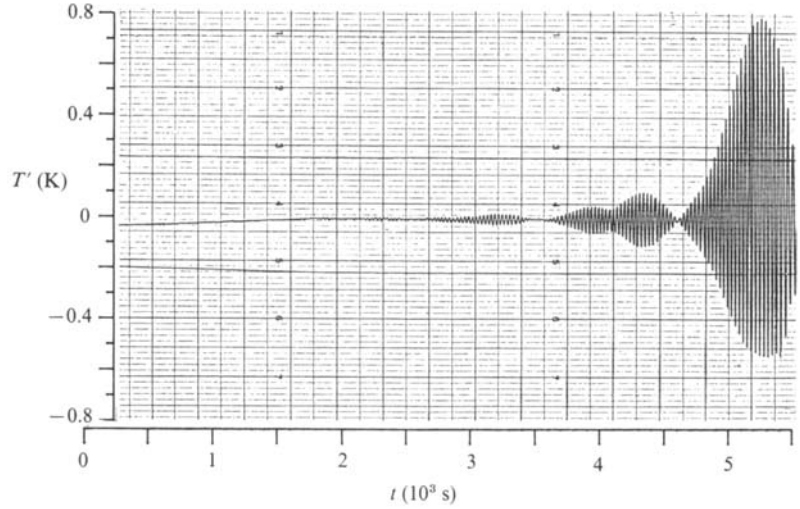

FIGURE 7. Signal of the temperature oscillation recorded by the thermocouple in the centre of the test apparatus, with initial concentration $C_0 = 15$ wt%, temperature difference across the layer $\Delta T = 26.02$ K, height ratio $A = 0.03$, and period $\tau = 29.3$ s.

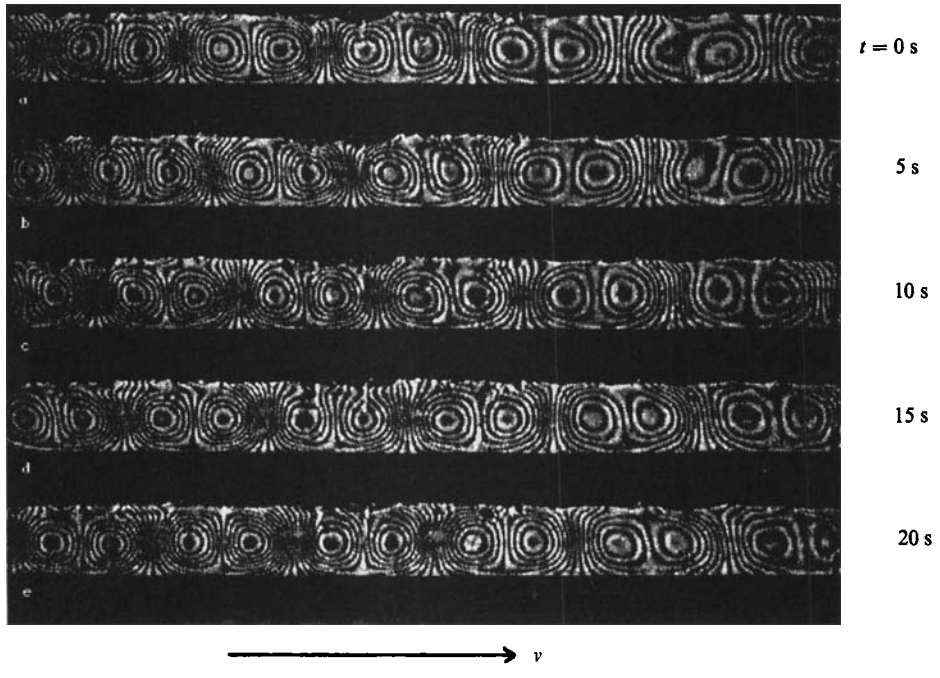

FIGURE 8. Set of interferograms recorded by a video camera at time intervals of $\Delta t = 5$ s. The interferograms show a modulated travelling wave for initial concentration $C_0 = 15$ wt%, temperature difference across the layer $\Delta T = 29.58$ K, height ratio $A = 0.10$, and period $\tau = 26.3$ s.

external temperature conditions, the period of time for individual rolls to cross the thermocouple is fixed. For the conditions in figure 7 the period is $\tau = 29.3$ s. An optical impression of the travelling wave mode is obtained from the sequence of interferograms in figure 8. The interferograms show a section near the centre of the test volume. The interferograms are taken at equal time intervals of $\Delta t = 5$ s.

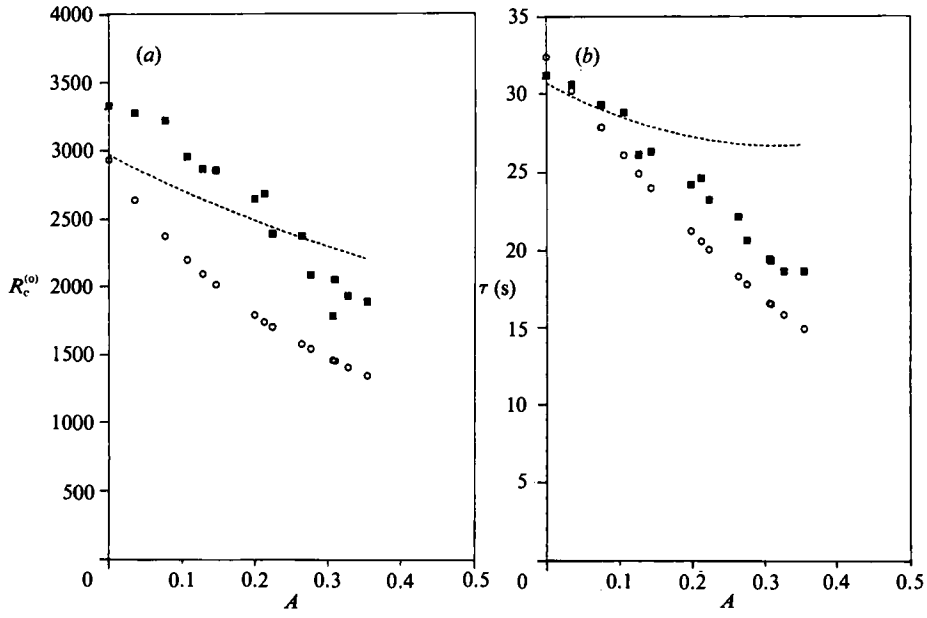

FIGURE 9. (*a*) Experimental (■) and calculated (○) values of the critical Rayleigh number as a function of the height ratio for initial concentration $C_0 = 15$ wt %; the dotted curve gives the effect of $\Psi(C)$ according to Lhost *et al.* (1991). (*b*) Experimental (■) and calculated (○) values of the oscillation period as a function of the height ratio, for $C_0 = 15$ wt %; the dotted curve gives the effect of $\Psi(C)$ according to Lhost *et al.* (1991).

The thickness of the ice layer is $h_s = 0.3 \pm 0.02$ mm and the temperatures at the boundaries are $T_0 = 19.20$ °C and $T_1 = -10.38$ °C, respectively. From the shift of the fringe patterns of consecutive interferograms the direction of propagation of the wave train from left to right is clearly recognized. Moreover, the growing density of the fringes from the right to the left side of each interferogram indicates increasing intensity of the convection due to amplification and/or modulation in time. A quantitative evaluation of the interferogram sequence gives a period of oscillation of $\tau = 26.3$ s. This value is also obtained from the chart record of the temperature fluctuations.

The onset of convection in the form of travelling waves is investigated systematically for different values of the ice thickness. For each thickness of the ice layer the critical temperature difference across the liquid layer at the onset of convection, and the period of the travelling wave are measured. From these measured values the critical Rayleigh number for onset of convection, the height ratio, and a dimensionless period τ of oscillation are evaluated. For the evaluation of the Rayleigh number one has to take into account that the concentration in the liquid phase increases with increasing thickness of the ice layer due to solute rejection. This in turn affects directly the melting temperature at the interface and some physical properties of the liquid such as the coefficient of thermal expansion. The material properties at mean temperatures of the liquid and solid phase are used for the evaluation of the dimensionless groups. The critical Rayleigh number and the dimensionless period of the travelling waves at onset of convection are plotted versus A in figure 9 (*a*, *b*). These plots show clearly that the critical Rayleigh number, as well as the period of the travelling wave motion, decrease with increasing ice-layer thickness.

For a comparison between experimental data and theoretical prediction the calculations of the critical parameters for onset of convection have been repeated for the particular conditions of the experiment. As input data of the experiment, the following quantities are used: $C_0 = 0.15$, $Pr = 30$, $Sc = 8900$, $St = 24.7$, $R_s = 173.4$, $S = -0.019$, $m = -14.4$. The calculated values R_{c0} and τ_0 are also shown in figure 9(*a*, *b*) together with the experimental data. The graphs show generally good agreement between the calculated and experimental curves. The monotonic decrease of the critical Rayleigh number with increasing thickness of the ice layer can be explained by the insulating effect of the ice at the upper boundary. An equivalent observation has been made by Davis *et al.* (1984) and by Dietsche & Müller (1985) in their experimental and theoretical investigations of a single-component liquid layers. There is, however systematic deviation between the curves in figure 9(*a*). The predicted Rayleigh numbers for the onset of travelling waves for all values of A considered are smaller than those of the experiments. The main reasons for this discrepancy are that (i) the experiments are carried out in a test volume with one lateral dimension relatively small, and (ii) the nonlinear density–temperature relation near the melting temperature T_s of the liquid makes the thermal expansion coefficient a strongly varying function of temperature. Our stability analysis assumes an infinitely wide layer and a linear density versus temperature relationship.

Figure 9(*b*) shows that the period of oscillation also decreases monotonically with increasing A. This behaviour is also readily explained on the basis of the linear stability theory. In liquid layers without ice the frequency of oscillation decreases when the Soret numbers decrease (see figure 4). In our case where the top of the layer is pure ice and the solute is completely rejected, the actual concentration of the liquid mixture beneath the ice is increased. Considering different static states for different ice-layer thicknesses, the increasing solute concentration affects the system as if S were replaced by $S(1+A)$. This can be immediately seen from the definition of the Soret coefficient $S_{\text{eff}} = SC(1-C)$ for $C \ll 1$. An effectively reduced Soret coefficient leads to higher oscillation frequencies.

When C is not so small, there is a significant dependence of the Soret coefficient on C as shown by Kolodner *et al.* (1988*c*). To estimate this influence on the critical Rayleigh number and the oscillation period we define the separation coefficient $\Psi = (a'/a) S_0 C_0 (1-C_0)$. For concentrations higher than 0.15 Kolodner *et al.* (1988*c*) found $\mathrm{d}\Psi/\mathrm{d}C = -3.8$ at $\Psi = -0.43$ or $C_0 = 0.15$. An increase of the ice layer causes an increase of the concentration in the liquid and therefore the separation coefficient changes to $\Psi(C) = \Psi(C_0) + \mathrm{d}\Psi/\mathrm{d}C(C_0)(C-C_0)$. To calculate the influence of a concentration dependence of the separation coefficient on R_c and τ_c the approximate formulae of Kolodner *et al.* (1988*b*) or of Lhost, Linz & Müller (1991) can be used. Both approximations are valid for small or zero Lewis numbers and their results differ by less than 1%. We have used equations (14)–(16) of Lhost *et al.* (1991) to calculate $R_c(A)$ and $\tau_c(A)$. The results are represented by the dotted lines in figure 9(*a*, *b*). It is shown that for $A = 0$ the approximate solution and our numerical solution agree quite well, within 2%. Increasing ice thickness leads to an additional decrease of R_c and τ_c due to increasing Ψ-values. For larger A, this effect is reflected in the stronger decrease of the experimental data compared with the calculated values. It is conjectured that the remaining discrepancy between the numerical and experimental values is mainly due to the finite geometry and the nonlinear density profile of the basic state.

When there is an ice layer at the upper boundary of the test volume, a permanent state of TW-convection is not observed. Whenever the amplitude of the temperature

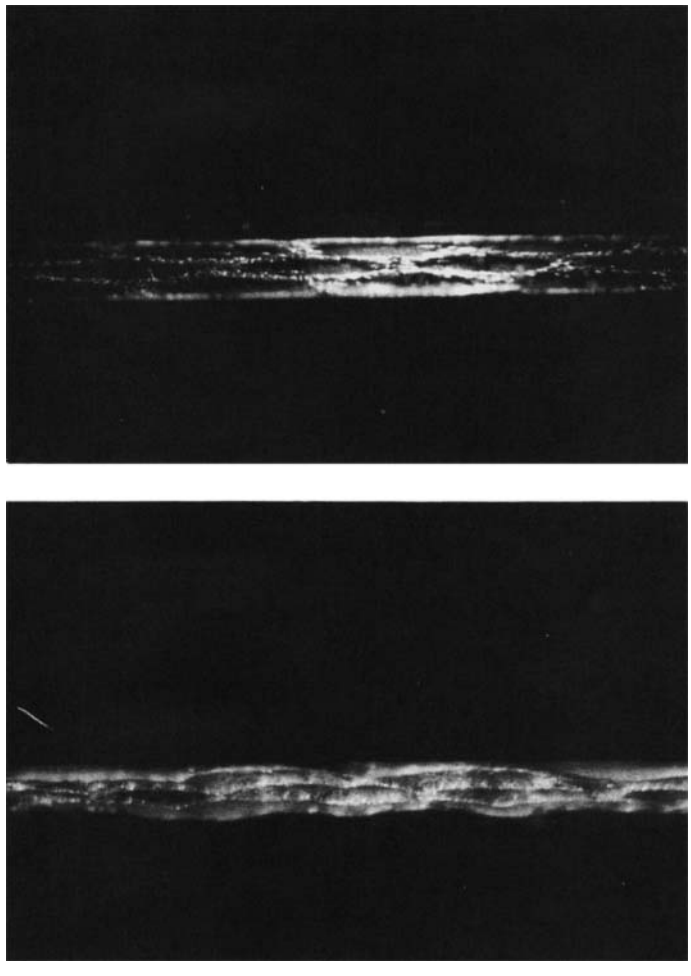

(*a*)

(*b*)

FIGURE 10. Photos of the ice surface at the upper boundary of the liquid layer taken by a steromicroscope with magnification (*a*) 5× and (*b*) 9×, respectively, with initial concentration $C_0 = 15$ wt%, and thicknesses of the ice layer (*a*) $A = 0$–0.03, (*b*) $A = 0.11$–0.18.

fluctuation near the ends of the test volume exceeds a threshold value, the travelling-wave motion in the cell dies out, starting from the cell ends. This is replaced by a three-dimensional steady convective pattern. The ice surface shows corrugations indicating polygonal cell structures of convection in the liquid. The two photos in figure 10 show typical examples for a thin and a moderately thick ice layer. The photos are taken with the aid of a stereomicroscope, which is focused on the ice surface from below at small angle of inclination. The magnifications are 5.3 and 8.8 for figure 10 (*a*, *b*) respectively. In the case of very thin ice layers, $h_S = 0.1$ mm, the copper surface is covered with isolated islands of ice separated by patches free of ice; the upflow melts the ice creating the patches, and the islands mark regions of downflow. Photos show the situation for an ice layer of thickness $h_S = 0.45$ mm. The deep, three-dimensional corrugations of the ice interface can be clearly seen. The pattern is stationary under fixed external boundary conditions within the test volume, except near the ends where slightly non-homogeneous temperature distributions give rise to local fluctuations of the cell boundaries.

4. Conclusions

Bénard convection of a two-component liquid is considered. The liquid displays Soret effects and the boundary temperatures are fixed to span the solidification temperature T_s of the mixture. Near the lower, heated plate the material is liquid and near the upper, cooled plate there is a layer of pure solid solvent; all the solute is rejected during freezing.

Linear stability theory is examined for the case of layers of infinite horizontal extent. The main parameters that occur are the thermal Rayleigh number R, the layer height ratio $A = h_S/h_L$, and the Soret coefficient S.

When there is no solid, $A = 0$, there is a critical value S^* of S with $S^* < 0$. When $S > S^*$ there is only steady convection, and when $S < S^*$ there are two branches of convection, one steady and one time periodic. The present calculations coincide with those of Chock & Li (1975) in this case. When solid is present, $A \neq 0$, there are modifications of S^*, R_c, the angular frequency ω_c and the wavenumber k_c. The tendencies of these changes are explained in physical terms.

Experiments are performed in a rectangular box of dimension $200 \times 20 \times 3.12$ mm. Mixtures of 15 wt% ethyl alcohol in water are used. The solid phase is pure ice from which all the alcohol has been rejected. Interferometry and photography are used to visualize the patterns and a thermocouple placed near the centre of the lower plate senses temperature fluctuations in the layer.

When ice is absent and the mean temperature $\bar{T}$ is sufficiently high, say $\bar{T} \approx 10$ °C, small, travelling-roll-cell perturbations are observed to vary slowly in their temperature intensities and move from one end of the test cell to the other. This state of modulated travelling waves is unstable for long times. Their amplitudes increase linearly with time and when they exceed a certain threshold value, the modulated travelling rolls settle down to a permanent state of travelling waves of constant amplitude. The state of permanent travelling waves exists only in a limited range of Rayleigh numbers in which the angular frequency decreases monotonically with increasing Rayleigh numbers. Moreover, there are two hysteretic jump transitions: (i) from the permanent state of travelling-wave motion to the steady state of overturning convection, and (ii) from the state of travelling-wave motion to the static state of heat conduction. These observations are in qualitative agreement with observations of Kolodner & Surko (1988), Fineberg *et al.* (1988*a*), Heinrichs *et al.* (1987) and Kolodner *et al.* (1988*a*, *b*) and with the theoretical predictions of Linz *et al.* (1988).

When ice is absent and the mean temperature is near enough to T_s, then Zimmermann (1990) and Zimmermann & Müller (1992) observe that the travelling waves do not represent a permanent state as they do at higher temperatures, but undergo a transition to steady (overturning) convection even for $S < S^*$. They attribute this change to the presence of nonlinear density–temperature profiles in the basic state.

When ice is present, the system undergoes the usual transitions to travelling-wave motion. This travelling-wave mode has critical values R_c, ω_c, k_c that are well described by our linear stability theory though there are systematic differences that are attributable to the presence of sidewalls in the cell and the effect of a nonlinear density–temperature distributions near T_s.

When ice is present, the travelling waves do not represent a permanent state as they do when $A = 0$ and the mean temperatures are high enough, but instead undergo a transition to steady convection even though $S < S^*$.

When the mean temperature $\bar{T}$ is sufficiently high, travelling waves are a permanent state. When it is near enough to T_s or the layer is partially solidified, the travelling waves do not persist but evolve to a stationary, polygonal, cellular pattern. There is no present theory for this behaviour though we conjecture here that it is due to the combined effects of the nonlinear density–temperature characteristic and the presence of the solid–liquid interface. Both of these act as non-Boussinesq effects on the nonlinear structure of the convection. A stationary three-dimensional cellular pattern has been observed by Dietsche (1984), Davis *et al.* (1984) and Dietsche & Müller (1985) in the case of pure fluid with partial solidification. The transition to a steady three-dimensional hexagonal flow is explained in their work by the coupling of interfacial corrugations with convection. Such corrugations have the same effect on pattern formation in steady convection as do other non-Boussinesq properties of a liquid (Davis & Segel 1968). The experiments of Zimmermann (1990) and Zimmermann & Müller (1992) in layers of mixtures of alcohol and water without ice show that at low mean temperatures only steady convection is a permanent state. At low temperatures the density of alcohol–water mixtures depends nonlinearly on the temperature. Such distributions also give rise to non-Boussinesq-like effects (see Krishamurti 1968). Recently, Hadji & Schell (1990) published the results of their nonlinear theory for a binary system coupled with a solid–liquid interface and a *positive* Soret coefficient. They found that near the convective threshold hexagons are the only stable states.

We conjecture, therefore, that Soret convection with significant non-Boussinesq effects will lead to steady (overturning) convection instead of the travelling-wave convection that is observed otherwise. In the present experiments the final convective state has polygonal structures that would presumably be hexagonal if the sidewalls were not as closely spaced as they are in the experiment.

Much of this work was performed at the Kernforschungszentrum Karlsruhe. U.M. gratefully acknowledges the hospitality shown during his visit to Northwestern University. We also acknowledge the valuable comments of a referee leading to improvements in the discussion. The authors wish to thank Ms. Crystal Martin and Ms. Judy Piehl for their creative typing. S.H.D. was supported by a grant from the National Aeronautics and Space Administration, Microgravity Science and Applications Program.

REFERENCES

AHLERS, G., CANNELL, D. S. & HEINRICHS, R. 1987 Convection in a binary mixture. *Nucl. Phys. B* (Proc. Suppl.) **2**, 77–86.

AHLERS, G. & LÜCKE, M. 1987 Some properties of an eight-mode Lorenz model for convection in binary fluids. *Phys. Rev.* A **35**, 470–473.

AHLERS, G. & REHBERG, I. 1986 Convection in a binary mixture heated from below. *Phys. Rev. Lett.* **56**, 1373–1376.

ANTAR, B. N. 1987 Penetrative double-diffusive convection. *Phys. Fluids* **30**, 322–330.

BENSIMON, D., KOLODNER, P., SURKO, C. M., WILLIAMS, H. & CROQUETTE, V. 1990 Competing and coexisting dynamical states of travelling-wave convection in an annulus. *J. Fluid Mech.* **217**, 441–467.

BRAND, H. R., LOMDAHL, P. S. & NEWELL, A. C. 1986 Benjamin–Feir turbulence in convective binary fluid mixtures. *Physica* **23D**, 345–361.

BRAND, H. R. & STEINBERG, V. 1984 Analog of the Benjamin–Feir instability near the onset of convection in binary fluid mixtures. *Phys. Rev.* A **29**, 2303–2304.

BÜHLER, K. 1979 Zellular Konvektion in rotierenden Behältern. *Fortschritt-Berichte der VDI-Zeitschriften*, Reihe 7, Nr. 54.

BÜHLER, K., KIRCHARTZ, K. R. & SRULIJES, J. 1978 Anwendung der Differentialinterferometrie bei thermischen konvektionsstromungen. In *Applied Fluid Mechanics* (ed. H. Oertel), pp. 54–69. Mitteil. Institüt für Strömungs lehre und Strömungsmaschinen, Universität Karlsruhe.

CALDWELL, D. R. 1970 Nonlinear effects in a Rayleigh–Bénard experiment. *J. Fluid Mech.* **42**, 161–175.

CALDWELL, D. R. 1973 Measurements of negative thermal diffusion coefficients by observing the onset of thermohaline convection. *J. Phys. Chem.* **77**, 2004–2008.

CALDWELL, D. R. 1974 Experimental studies on the onset of thermohaline convection. *J. Fluid Mech.* **64**, 347–367.

CALDWELL, D. R. 1975 Soret coefficient of 1N lithium iodide. *J. Phys. Chem.* **79**, 1882–1884.

CALDWELL, D. R. 1976 Thermosolutal convection in a solution with large negative Soret coefficient. *J. Fluid Mech.* **74**, 129–142.

CHOCK, D. P. & LI, C.-H. 1975 Direct integration method applied to Soret-driven instability. *Phys. Fluids* **18**, 1401–1406.

CROSS, M. C. 1986*a* An eight-mode Lorenz-model of travelling waves in a binary fluid convection. *Phys. Lett.* A **119**, 21–24.

CROSS, M. C. 1986*b* Travelling and standing waves in binary-fluid convection in finite geometries. *Phys. Rev. Lett.* **57**, 2935–2938.

CROSS, M. C. 1988 Structure on nonlinear travelling-wave states in finite geometries. *Phys. Rev.* A **38**, 3593–3600.

CROSS, M. C. & KIM, K. 1988 Linear instability and the codimension-2 region in binary fluid convection between rigid impermeable boundaries. *Phys. Rev.* **137**, 3909–3920.

D'AN-LAX, E. 1967 *Taschenbuch für Chemiker und Physiker*, vol. 1 (Third Edn). Springer.

DAVIS, S. H., MÜLLER, U. & DIETSCHE, C. 1984 Pattern selection in single-component systems coupling Bénard convection and solidification. *J. Fluid Mech.* **144**, 133–151.

DAVIS, S. H. & SEGEL, L. A. 1968 Effects of surface curvature and property variation on cellular convection. *Phys. Fluids* **11**, 470–476.

DEANE, A. E., KNOBLOCH, E. & TOOMRE, J. 1988 Travelling waves and chaos in large-aspect-ratio thermosolutal convection. *Phys. Rev.* A **37**, 1817–1820 and Erratum, *Phys. Rev.* A **38**, 1661 (1988).

DEGROOT, S. R. & MAZUR, P. 1969 *Non-equilibrium Thermodynamics* (2nd edn). North-Holland.

DIETSCHE, C. 1984 Einfluss der Bénard-Konvektion auf Gefrierflachen. *KfK-Bericht* 3724.

DIETSCHE, C. & MÜLLER, U. 1985 Influence of Bénard convection on solid–liquid interfaces. *J. Fluid Mech.* **161**, 249–268.

FINEBERG, J., MOSES, E. & STEINBERG, V. 1988*a* Spatially and temporally modulated travelling-wave pattern in convecting binary mixtures. *Phys. Rev. Lett.* **61**, 838–841.

FINEBERG, J., MOSES, E. & STEINBERG, V. 1988*b* Nonlinear pattern and wave-number selection in convecting binary mixtures. *Phys. Rev.* A **38**, 4939–4942.

FINEBERG, J. & MOSES, E. & STEINBERG, V. 1989 Reply to: P. Kolodner (1989). *Phys. Rev. Lett.* **64**, 579.

GRAUER, T. & HAKEN, H. 1988 Generalized Ginzberg–Landau equations applied to instabilities in systems coupling convection and solidification. In *Physicochemical Hydrodynamics, Interfacial Phenomena* (ed. M. G. Velarde). NATO ASI Series, Vol. 174, pp. 571–582. Plenum.

HADJI, L. & SCHELL, M. 1990 Soret-driven convection coupled to the morphology of a solid–liquid interface. *Phys. Fluids* A **2**, 1597–1606.

HEINRICHS, R., AHLERS, G. & CANNELL, D. S. 1987 Travelling waves and spatial variations in the convection of a binary mixture. *Phys. Rev.* A **35**, 2761–2764.

HURLE, D. T. J. & JAKEMAN, E. 1969 Significance of the Soret effect in the Rayleigh–Jeffreys problem. *Phys. Fluids* **12**, 2704–2705.

HURLE, D. T. J. & JAKEMAN, E. 1971 Soret-driven thermosolutal convection. *J. Fluid Mech.* **47**, 667–687.

HURLE, D. T. J. & JAKEMAN, E. 1973*a* Thermal oscillations in convecting fluids. *Phys. Fluids* **16**, 2056–2059.

HURLE, D. T. J. & JAKEMAN, E. 1973*b* Natural oscillations in heated fluid layers. *Phys. Lett.* **43A**, 127–129.

KIRCHARTZ, K.-R. 1980 Zeitabhangige zellularkonvektion in horizontalen und geneigten behaltern. Dissertation an der Universitat Karlsruhe.

KNOBLOCH, E. & MOORE, D. R. 1988 Linear stability of experimental Soret convection. *Phys. Rev.* A **37**, 860–870.

KOLODNER, P., BENSIMON, D. & SURKO, C. M. 1988*a* Travelling-wave convection in an annulus. *Phys. Rev. Lett.* **60**, 1723–1726.

KOLODNER, P., PASSNER, A., SURKO, C. M. & WALDEN, R. W. 1986 Onset of oscillatory convection in a binary fluid mixture. *Phys. Rev. Lett.* **56**, 2621–2624.

KOLODNER, P., PASSNER, A., WILLIAMS, H. L. & SURKO, C. M. 1987*a* The transition to finite-amplitude travelling-wave convection in binary fluid mixtures. *Nucl. Phys.* B (Proc. Suppl.) **2**, 97–108.

KOLODNER, P. & SURKO, C. M. 1988 Weakly nonlinear travelling-wave convection. *Phys. Rev. Lett.* **61**, 842–845.

KOLODNER, P., SURKO, C. M., PASSNER, A. & WILLIAMS, H. L. 1987*b* Pulses of oscillatory convection. *Phys. Rev.* A **36**, 2499–2502.

KOLODNER, P., SURKO, C. M., WILLIAMS, H. L. & PASSNER, A. 1988*b* Two-frequency states at the onset of convection in binary fluid mixtures. In *Propagation in Systems Far From Equilibrium* (ed. J. E. Wesfreid, H. R. Brand, P. Manneville, A. Albinet, and N. Boccara), pp. 282–291. Springer.

KOLODNER, P., WILLIAMS, H. & MOE, C. 1988*c* Optical measurement of Soret coefficient of ethanol/water solutions. *J. Chem. Phys.* **88**, 6512–6524.

KRISHNAMURTI, R. 1968 Finite amplitude convection with changing mean temperatures. *J. Fluid Mech.* **33**, 445–455.

KURZ, W. & FISHER, D. J. 1989 *Fundamentals of Solidification*. Switzerland: Trans. Tech. Publications.

LEGROS, J. C., PLATTEN, J. K. & POTY, P. G. 1972 Stability of a two-component fluid layer heated from below. *Phys. Fluids* **15**, 1383–1390.

LEGROS, J. C. & PLATTEN, K. 1977 Two-component Bénard problem with Poiseuille flow. *J. Non-Equilib. Thermodynam.* **2**, 211–232.

LHOST, O., LINZ, S. J. & MÜLLER, H. W. 1991 Onset of convection in binary liquid mixtures: Improved Galerkin approximations. *J. Phys.* II **1**, 279–287.

LHOST, O. & PLATTEN, J. K. 1988 Transitions between steady states, travelling waves and modulated travelling waves in the system water–isopropanol heated from below. *Phys. Rev.* A **38**, 3147–3150.

LHOST, O. & PLATTEN, J. K. 1989 Experimental study of the transition from nonlinear travelling waves to steady overturning convection in binary mixtures. *Phys. Rev.* A **40**, 4552–4557.

LINZ, S. J. & LÜCKE, M. 1987 Convection in binary mixtures: A Galerkin model with impermeable boundary conditions. *Phys. Rev.* A **35**, 3397–4000.

LINZ, S. J., LÜCKE, M., MÜLLER, H. W. & NIEDERLANDER, J. 1988 Convection in binary fluid mixtures: Travelling waves and lateral currents. *Phys. Rev.* A **38**, 5727–5741.

MOSES, E., FINEBERG, J. & STEINBERG, V. 1987 Multistability and confined travelling-wave patterns in a convecting binary mixture. *Phys. Rev.* A **35**, 2757–2760.

MOSES, E. & STEINBERG, V. 1986 Flow patterns and nonlinear behavior of travelling waves in a convective binary fluid. *Phys. Rev.* A **34**, 693–696 and Erratum. *Phys. Rev.* A **35**, 1444–1445 (1987).

MOSES, E. & STEINBERG, V. 1988 Mass transfer in propagating patterns of convection. *Phys. Rev. Lett.* **60**, 2030–2033.

OTT, J. B., GOATES, J. R. & WAITE, B. A. 1979 (Solid–liquid) phase equilibria and solid–hydrate formation in water + methyl + ethyl + isopropyl, and + terciary butyl alcohols. *J. Chem. Thermodyn.* **11**, 739–746.

PLATTEN, J. K. 1971 Le probleme de Bénard dans les Melanges: cas de surface libres. *Bull. Classe Sci. Acad. Roy. Belg.* **57**, 669–683.

PLATTEN, J. K. & CHAVEPEYER, G. 1972*a* Oscillations in a water–ethanol liquid layer heated from below. *Phys. Lett.* **40A**, 287–288.

PLATTEN, J. K. & CHAVEPEYER, G. 1972*b* Soret driven instability. *Phys. Fluids* **15**, 1555–1557.

PLATTEN, J. K. & LEGROS, J. C. 1984 *Convection in Liquids*. Springer.

REHBERG, I. & AHLERS, G. 1986 Codimension-two bifurcation in a convection experiment. *Contemp. Maths* **56**, 277–282.

ROSENBERGER, F. 1979 *Fundamentals of Crystal Growth I*. Springer.

SCHECHTER, R. S., PRIGOGINE, I. & HAMM, J. R. 1972 Thermal diffusion and convective stability. *Phys. Fluids* **15**, 379–386.

SCOTT, M. R. & WATTS, H. A. 1975 Subroutine SUPORT. *Rep.* SAND75-0198. Saudia Labs Albuquerque.

SORET, M. CH. 1879 Une dissolution saline primitivement homogene. *Arch. Sci. Phys. Nat. Geneve* **2**, 48–61.

STEINBERG, V. & MOSES, E. 1987 Experiments on convection in binary mixtures. In *Pattern, Defects and Microstructures in Nonequilibrium Systems, Proc. NATO Advanced Research Workshop* (ed. D. Walgraef). NATO ASI Series, pp. 309–335. Martinus Nijhoff.

STEINBERG, V., MOSES, E. & FINEBERG, J. 1987 Spatio-temporal complexity at the onset of convection in a binary fluid. *Nucl. Phys.* B (Proc. Suppl.) **2**, 109–124.

SULLIVAN, T. S. & AHLERS, G. 1988*a* Hopf bifurcation to convection near the codimension-two-point in a ^{3}He-^{4}He mixture. *Phys. Rev. Lett.* **61**, 78–81.

SULLIVAN, T. S. & AHLERS, G. 1988*b* Nonperiodic time dependence at the onset of convection in a binary liquid mixture. *Phys. Rev.* A **38**, 3143–3146.

SURKO, C. M., KOLODNER, P., PASSNER, A. & WALDEN, R. W. 1986 Finite-amplitude travelling-wave convection in binary fluid mixtures. *Physica* **23D**, 220–229.

VILLERS, D. & PLATTEN, J. K. 1984 Heating curves in the two-component Bénard problem. *J. Non-Equilib. Thermodyn.* **9**, 131–146.

WALDEN, R. W., KOLODNER, P., PASSNER, A. & SURKO, C. M. 1985 Travelling waves and chaos in convection in binary fluid mixtures. *Phys. Rev. Lett.* **55**, 496–499.

ZIELINSKA, B. J. A. & BRAND, H. R. 1987 Exact solution of the linear-stability problem for the onset of convection in binary fluid mixtures. *Phys. Rev.* A **35**, 4349–4353 and Erratum. *Phys. Rev.* A **37**, 1786 (1988).

ZIMMERMANN, G. 1990 Bénard-Konvektion in binaren Flüssigkeitsmischungen mit thermo-diffusion. *KfK-Bericht* 4683.

ZIMMERMANN, G. & MÜLLER, U. 1992 Bénard convection in binary mixtures with Soret effects. *Intl J. Heat Mass Transfer* **35** (in press).

ZIMMERMANN, G., MÜLLER, U. & DAVIS, S. H. 1986 Bénard convection in a partly solidified two-component system. *KfK-Bericht* 4122.